Chapter 4

Nanofluidics

4.1 Introduction

Research on nanofluidics has expanded rapidly because it enables one to observe novel scientific phenomena in fluid dynamics occurring in unexplored dimensions, and also covers some features that can be utilized for various applications.

Nanofluidic channels in the form of cell membrane ion channels, such as α-hemolysin, were first used in the 1990s to detect DNA and RNA (1). By applying a voltage across these channels, DNA and RNA molecules were drawn through as extended linear chains. Their presence detectably reduced normal ionic flow through the nanochannels, and it was possible to characterize the length of the polymers and even small portions of their sequences (2). Recently, fabricated inorganic nanochannels have gained preference over the biological membrane channels due to better control over channel dimensions and surface characteristics (3-6).

Most of these conduits have been made of silica, a material which has allowed nanochannels to exhibit interesting phenomena in the presence of aqueous solutions. In aqueous solutions, water reacts with silica to form silanol groups, as shown in following reaction:

$$H_2O + \equiv Si—O—Si\equiv \rightarrow \equiv Si—OH + HO—Si\equiv$$

In most cases, water is a little acidic at pH ~ 6, whereas the pK_a of silica is between 2 and 4.5. Therefore, when exposed to water, the silanol groups become deprotonated, resulting

in the formation of negative charges on the surface of the silica. In the presence of ionic solutions, positively-charged counter-ions accumulate next to the channel surface, effectively shielding the negative surface charge over a distance called the Debye length (7). The dimensions of conventional microfluidic channel devices far exceed this characteristic length, therefore the surface charge has a negligible effect upon the distribution of ions in solutions flowing inside. However, the width and height of nanofluidic channels can be on the order of the Debye length, allowing the surface charge to have a dominating effect on ion distributions within the nanochannels (6, 8).

Advantages of nanofluidic devices are multifold. First, nanofluidic devices enable electrical and optical detection at the same time. The movement of the target molecules attached to a fluorescent dye may be tracked optically. Even without optical monitoring, binding of the target molecule on the surface of the channel or transport of relatively large molecules may be detected electrically. Because surface charge dominates ionic conductance when the Debye length exceeds the channel dimensions (9, 10), reactions or other molecular events that change the channel surface charge can be detected electrically. Also, as the size of target molecules is comparable to the channel dimensions, transport of the target molecules could be electrically detected due to excluded volume effect (3). Second, nanofluidic devices can be used to separate molecules, as an alternative to gel methods, but with better resolution. Obviously, the nanofluidic devices will block molecules larger than the channel dimensions, allowing only smaller molecules to pass through. Furthermore, by utilizing electrostatic interactions between the molecules and the nanofluidic channel surface, the nanofluidic devices can distinguish molecules based on their charges. Han and colleagues developed 2-D nanofluidic arrays to separate DNA

and proteins based upon their lengths and isoelectric points (11). They reported on the anisotropic nanofilter array (ANA), which is a unique filtering platform that incorporates various sieving mechanisms such as Ogston sieving, entropic trapping and electrostatic sieving. Third, one-dimensional geometry with a cross-section that is on the order of macromolecular dimensions provides for a unique environment. Most polymers whose radius of gyration is larger than channel diameter could be stretched out along the channel. This stretching can be a useful tool for studying the importance of molecular structure in various reactions. Austin and his colleagues delivered lambda-DNA and restriction enzymes to the nanochannels, and then observed site-specific positions where nucleotides were digested by these restriction enzymes at single molecule resolution. Finally, confined environments mimic real intracellular conditions where only nanometer-size pores, supported in a matrix of between impermeable molecules, are available for molecular transport. Investigating biological reactions in such cell-like conditions might be helpful for predicting their kinetics and equilibrium in real cell environments.

Taking advantage of the capability of fabricating nanowire arrays, I have initiated a nanofluidic project starting in the summer of 2006. The near-term goal of the project is to detect and separate peptides based on their isoelectric points. Although the project is still in the development stage, many promising results have been produced and I expect that the device will find a host of applications in biomolecule sensing. In this chapter, I will introduce the device fabrication procedures, progresses to date and future directions.

4.2 Device Fabrication

The first step in building nanochannels was to generate a nanowire template. The SNAP method (12) and standard electron beam lithography (EBL) were used to make an array of silicon nanowires on a transparent quartz substrates. The detailed procedures of the SNAP method are described in subchapter 3-2. In the silicon nanowire array generated by the SNAP method, each wire was about 15 - 20nm wide and 50 nm apart from adjacent wires. The wires were sectioned into regions about 25 μm in length and 5 μm in width by standard electron beam lithography (EBL). The standard EBL procedures used here were the same as in the fabrication of 160 kbit molecular electronic memory devices (see subchapter 3-4). Low Pressure Chemical Vapor Deposition (LPCVD) was then used to deposit a 5 μm thick silicon dioxide layer on top of and between the wires according to the reaction: $SiH_4 + O_2 \rightarrow SiO_2 + 2H_2$. Photoresist was spun onto the low temperature oxide (LTO) layer and a microchannel pattern was made by photolithography. The pattern was etched down via an Active Oxide Etching (AOE) process (CHF_3:C_4F_8:Ar = 33 sccm:7 sccm:10 sccm, 200 W, 10 mTorr, 15 minutes) to expose the ends of the SNAP wires (figure 4-1a). This gave a set of microchannels connecting either end of the SNAP wires. The microchannel depth that was about 5.5 μm was confirmed by a surface profiler (Dektak 150), and then the photoresist was striped by acetone. The substrate was further cleaned by a piranha solution (H_2SO_4: H_2O_2 = 3:1 by volume). At this point, XeF_2 was used to selectively and isotropically etch the silicon wires to form hollow channels within the glass according to the reaction: $2XeF_2 + Si \rightarrow SiF_4(g) + 2Xe(g)$, as shown in figure 4-1b. Before loading substrates into the XeF_2 etching chamber, the substrates were dipped into a buffered oxide etching (BOE:

NH_4F/HF= 6:1 by volume) solution very quickly to remove native oxide layers on the channel entrances. The pressure of XeF_2 gas was maintained at about 2800 mTorr during the etching procedures. In most cases, the etching progress was confirmed by a color change in optical microscope images.

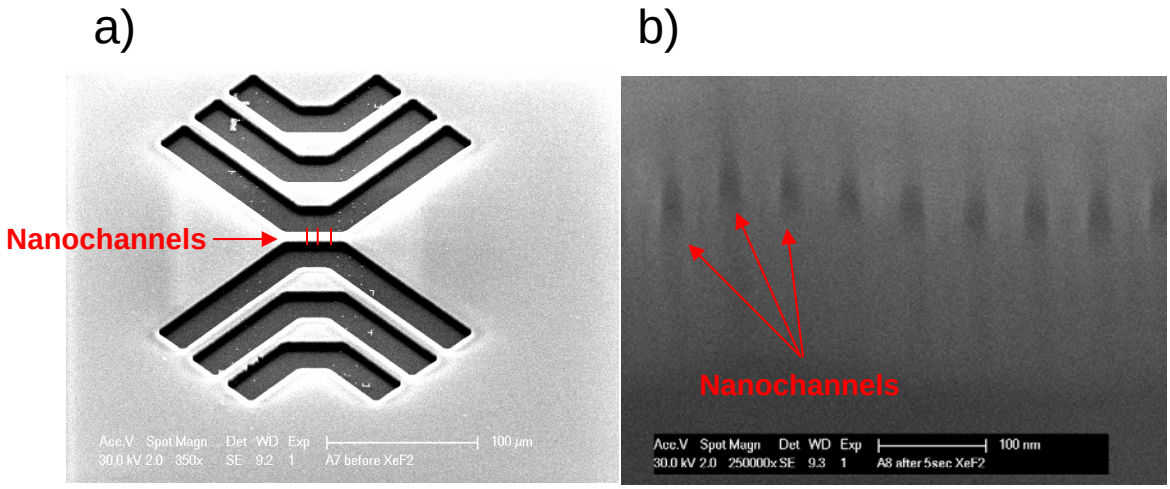

Figure 4-1. Scanning electron micrograph (SEM) images of nanofluidic devices. (a) Microchannels are anisotropically etched into the LTO layer, exposing the ends of the SNAP wires. As indicated by the arrow, the nanochannels bridge both sides of the microchannels (b) XeF_2 etches away the SNAP wires to create nanochannels. The nanochannel entrances are indicated. The channel height appeared to wander due to imaging artifacts.

Finally, PDMS with drilled input/output holes was bonded to the device by using an oxygen plasma technique to create a watertight seal between the microchannels. This seal ensures that the only connection between the microchannels is via the nanochannels. Ionic and biological solutions were inserted through the input holes in the PDMS, and the ionic current measurements were done with the use of a source/preamplifier unit (Keithley 2400) (figure 4-2a). Commercially available Ag/AgCl electrode assemblies (E. W. Wright) were used as electrodes. The ensuing electrophoretic current can be read,

thereby allowing the characterization of ionic and biological transport through the nanochannels.

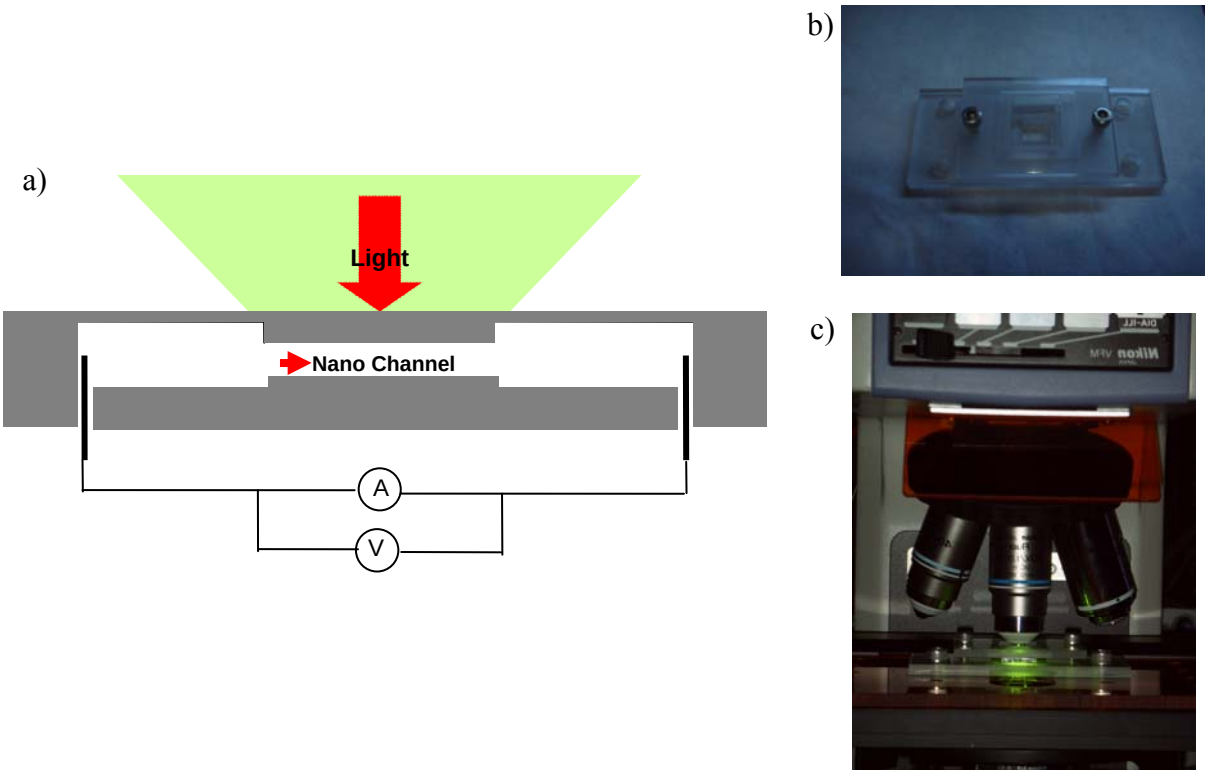

Figure 4-2. Nanofluidic device and characterization set-up. (a) Schematic illustration of the nanofluidic device and the measurement set-up. Optical and electrical measurements are carried out simultaneously. (b) A device holder was designed to flip the device over for microscope imaging and to prevent leakage between glass substrate and PDMS cover. (c) Fluorescence microscope used for optical characterization. A nanofluidic device located in the holder is visualized by fluorescence microscopy.

4.3 Toward Single-Molecule Chemical Filters

As introduced in the previous subchapters, delicate fabrication techniques allow one to routinely generate the nanochannels whose dimensions are smaller than the Debye screening length. Within this regime, target molecules delivered to the nanochannels are under electrostatic interaction with the nanochannel wall. Therefore, molecules with

different charges might produce different diffusivities, and thus the devices could function as novel type of columns separating molecules based on their charges. Obviously, the idea could be expanded to a variety of molecules such as peptides, polymers and even small molecules.

At low ionic strength, counter-ions are electrostatically attracted by the nanochannel wall, whereas co-ions are repelled because electroneutrality should be satisfied in the nanochannel. Therefore, the nanochannel could be filled with unipolar ions. The unipolar environment makes the nanofluidic system deviate from a bulk solution system where bipolar ionic transport is general at all ionic strengths. In the bipolar regime, the resistance of ionic transport relies on the channel geometry being inversely proportional to the channel cross-section. In case of the unipolar regime, however, the surface charge has an additional effect to attract the counter-ions. Therefore, the ionic transport in the nanochannel should be analyzed separately for co-ions and counter-ions. For clarity, I assign co-ions and counter-ions to negative and positive ions, respectively, because silica is the most common channel material and is negatively charged in contact with aqueous solution.

Now the case where bias is applied through the nanochannel is considered. The negative ions are depleted from the nanochannel region due to the electrostatic repulsion until a bias larger than the nanochannel potential barrier is applied. On the other hand, for the positive ions, a voltage drop along the nanochannel is still valid. But, the density of positive ions in this unipolar regime turns out to increase by order of magnitudes (13, 14). Consequently, the net effect of the nanochannel is a significant increase in ionic flux compared to the bipolar ionic transport where the channel cross-section is the only

parameter contributing to the ion flux. In summary, at low ionic concentration, the channel surface charge dominates the ionic flux in the nanochannel and thereby breaks down the continuity of electric potential for ions of each polarity.

Using fluorescent dyes, the experiment was performed to test the unipolar characteristic of the nanochannel. It was confirmed that with the dyes used herein, fluorescence intensity is linearly proportional to their concentration. Hence, diffusion characteristics for these dyes could be obtained by measuring the fluorescence intensity with respect to time. The fluorescence images were obtained by a fluorescence microscope with a 60x objective (Nikon Fluor) and a 1.0 numerical aperture. The excitation of the fluorophore was performed with a mercury lamp (Nikon super high pressure, C-SHG1) and images were taken with a cooled CCD camera (Hamamatsu, ORCA-ER).

For clear dye tracking, nanochannels about 4 μm wide were defined by EBL. Before the dye loading, potassium chloride (KCl) solution at low ionic strength (10 μM) was inserted into both sides of the microchannel. Under this background ionic strength in conjunction with concentration of target molecules (~ 10 μM in most cases), the Debye screening length is expected to be ~ 60 nm. Therefore the nanochannel thickness (~ 35 nm) is smaller than the Debye screening length. The nanochannel wets mainly by the capillary phenomenon and the wetting progress was monitored optically and electrically (figure 4-3). Once the nanochannels are filled with the KCl solution completely, the ionic conductance increases significantly from a noise level to a substantial level, forming linear ohmic IV traces (figure 4-3a). At this point, a drop of dye was located in the inlet of the PDMS and diffusion was monitored thereafter.

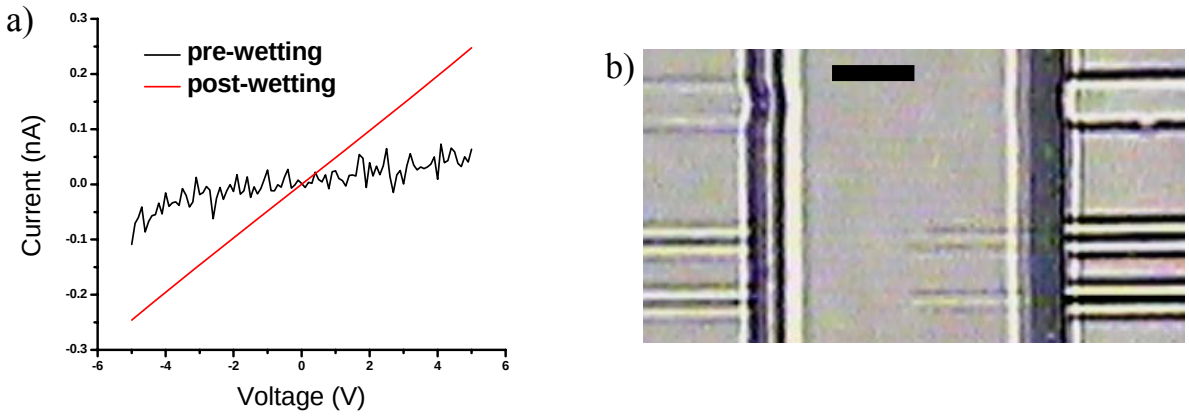

Figure 4-3. Nanochannel wetting progress. (a) Conductance across the nanochannel was monitored throughout the wetting process. Once the nanochannels wetted, the current increased significantly. (b) A bright-field image of the nanochannels during the wetting progress. The uppermost wide channel wets completely, whereas two bottom channels wet halfway. Scale bar is 5 μm.

Result and Discussion

First, cationic and anionic dyes were tested for transport through the nanochannels. Sulforhodamine 101 cadaverine (Anaspec) and fluorescein isothiocyanate (FITC) (Sigma-Aldrich) were used as cationic and anionic dyes, respectively. Fluorescence images of those dyes at different time are presented in figures 4-4 and 4-5, alongside their molecular structures and fluorescence intensity data.

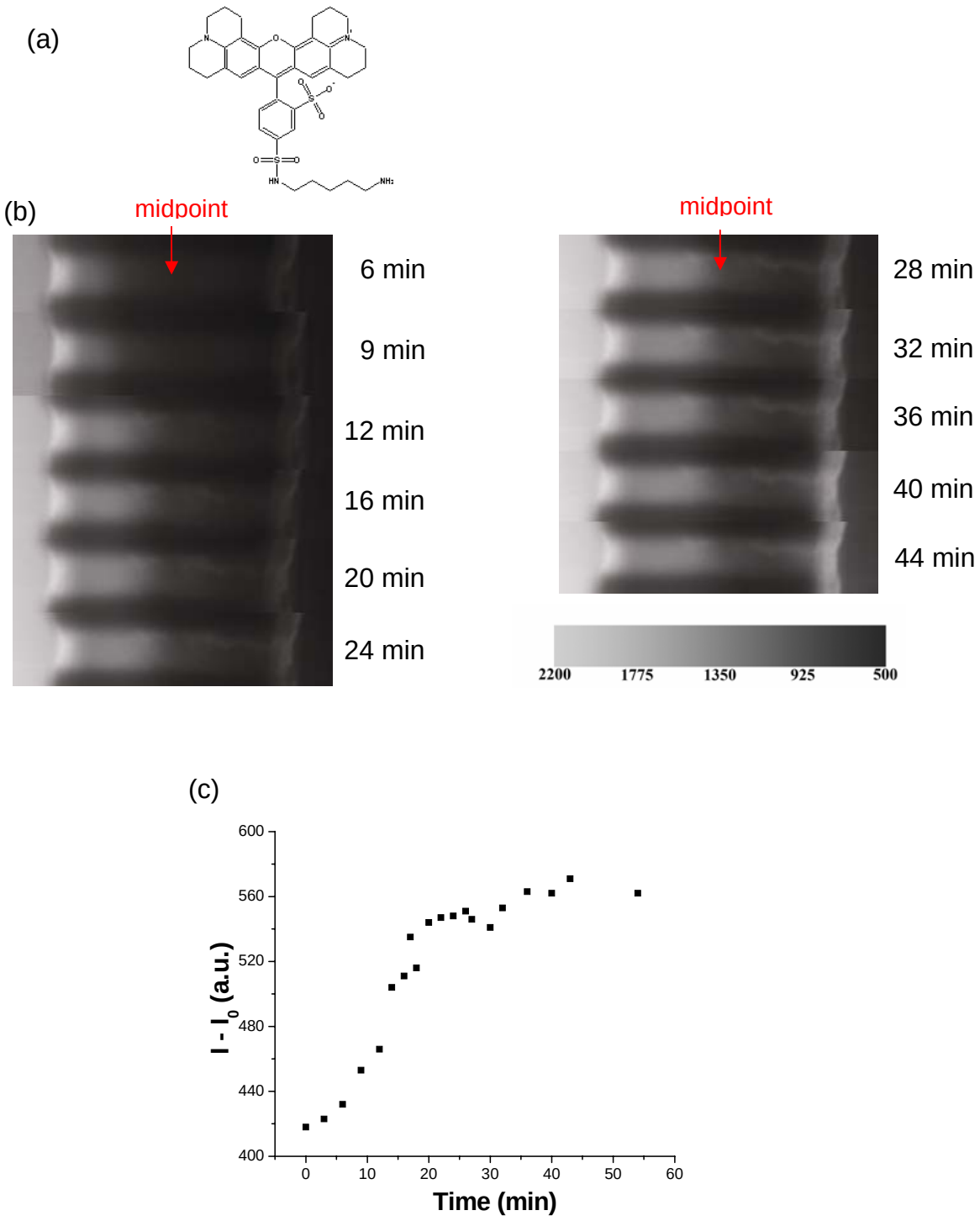

Figure 4-4. Diffusion of a cationic dye. (a) Molecular structure of Sulforhodamine 101 cadaverine used as a cationic dye. (b) Fluorescence images over the nanochannel regions taken during the diffusion of the cationic dye. The channel width is about 4 μm. (c)

Background subtracted fluorescence intensity at the midpoint of the nanochannel shown in (b).

(a)

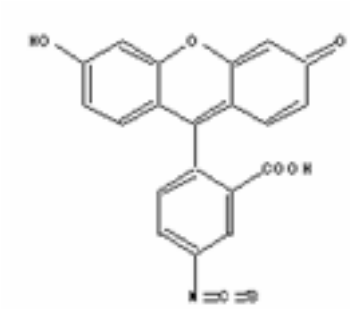

(b)

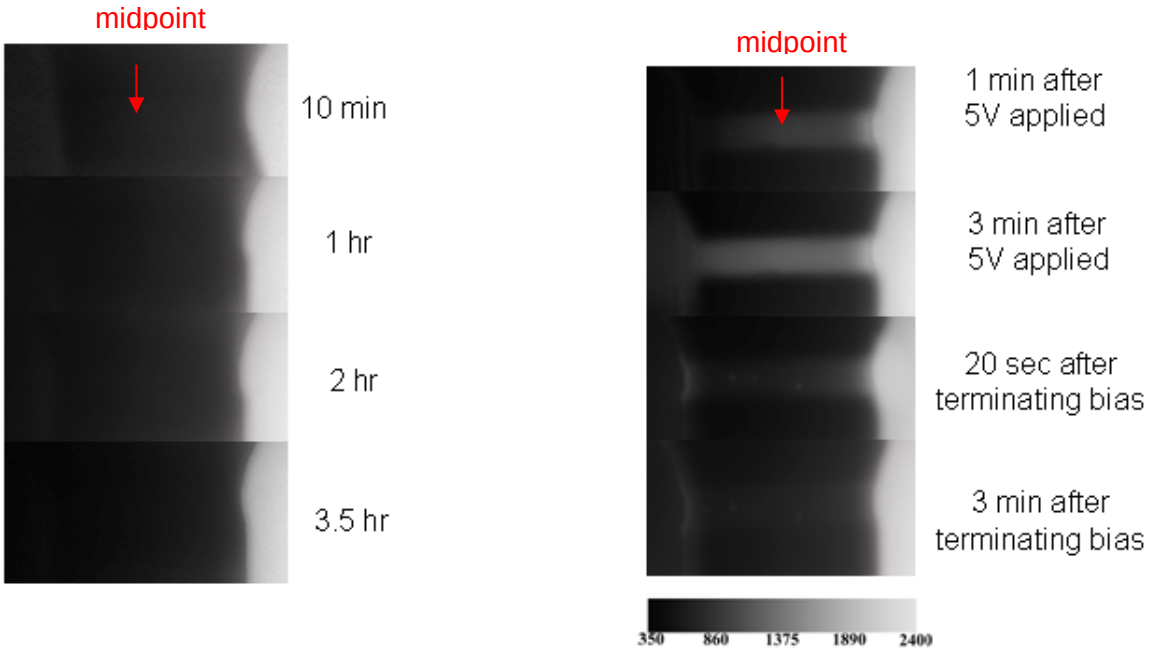

(c)

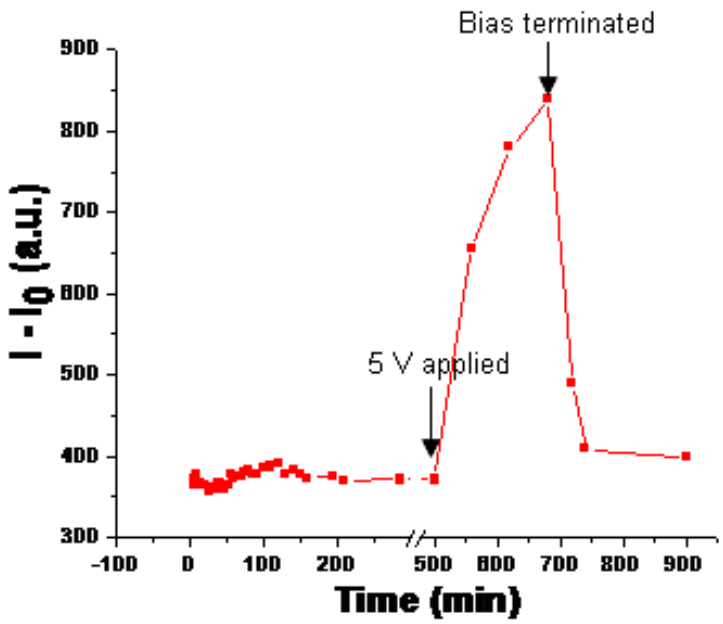

(d)

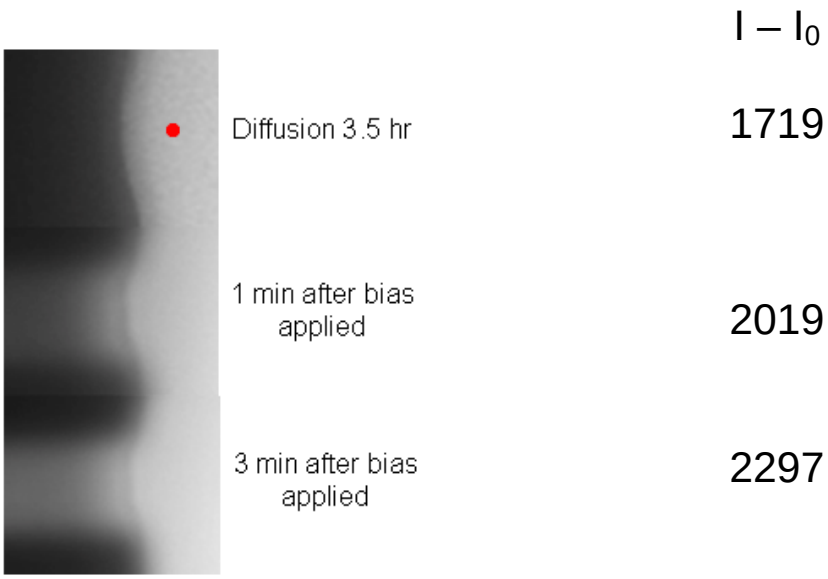

Figure 4-5. Diffusion of an anionic dye. (a) Molecular structure of fluorescein isothiocyanate (FITC) used as an anionic dye. (b) Fluorescence images over the nanochannel regions taken during the diffusion and bias application. The channel width is about 4 μm. (c) Background subtracted fluorescence intensity at the midpoint of the nanochannel shown in (b). (d) High-resolution fluorescence images at the interface

between the nanochannel and the right microchannel. Background subtracted fluorescence intensities measured at the indicated point in the fluorescence image are also presented. Increased fluorescence intensity at the interface indicates a local dye accumulation due to the potential energy barrier.

Several things are noticeable from these diffusion data for the dyes carrying different charges.

First, as expected from the electrostatic interactions, the cationic and anionic dyes showed apparent difference in the diffusion efficiency. The fluorescence intensity by the cationic dye increased gradually with time, whereas little or no diffusion was observed for the anionic dye, though measured over a longer period (> 3 hours). Again, the opposite diffusion trends between these dyes are indicative of the unipolar condition inside the nanochannel where the positive ions are dominant. In particular, the impaired diffusion of the anionic dye suggests significant potential barrier originated from the negative surface charge.

Second, in the case of anionic dye, the external bias could modulate the ionic transport. As +5 V was applied to the left microchannel, the ionic transport of the anionic dye was enabled and clear fluorescence intensity appeared in the nanochannel. This phenomenon is illustrated in the image taken at one minute after the bias was held to the left microchannel (figure 4-5b). At this moment, it was likely that the front end of the dye was passing the 4/5 point of the nanochannel and continuously moving toward the left microchannel. The image taken after 3 minutes of the bias application shows clearly that the dye diffused through the nanochannel. The source of the electrophoretic ionic flux lies in the fact that the external bias can overcome the electric potential barrier generated by the nanochannel surface charges. Fluorescence images were taken even after the

external bias was terminated, and interestingly, the anionic dyes were drained from the nanochannel immediately (two lowermost images in the right panel of figure 4-5b). The image taken 20 seconds after terminating the bias shows a slightly higher fluorescence intensity at the interface between the nanochannel and the right microchannel due to the dye molecule draining. The immediate draining of the dye from the nanochannel also reflects the potential barrier inside the nanochannel. The fact that the nanochannel looks brighter than before the bias was applied might be due to adsorbed dyes during the bias-driven electropheretic transport. A similar bias application measurement was performed for the cationic dye as a subsequent experiment to what is shown in figure 4-4. After the cationic dye diffused through to the right microchannel (same orientation as figure 4-4), -5 V was applied to the left channel with the intention of attracting the cationic dye back toward the left side. An apparent fluorescence intensity decrease was observed on the right microchannel suggesting the electrophoretic movement of the cationic dye in the opposite direction to the diffusion (data not shown). However, the intensity decrease during the bias application was not as steep as with the anionic dye, perhaps due to low fluorescence intensity at the initial point of the bias application.

Third, in case of the anionic dye, a dye accumulation related to the local potential barrier was observed at the interface between the nanochannel and the right microchannel upon the bias application. High-resolution fluorescence images focusing on the interface are presented in figure 4-5d. As indicated by the background subtracted fluorescence intensity, the fluorescence intensity at the interface increased upon the bias application. This increase suggests that while the dyes are electrophoretically driven toward the left

microchannel, they are accumulated locally at the interface due to the potential barrier related to the nanochannel surface charge.

Finally, diffusivity (D) of the cationic dye may be approximately estimated by $D \sim l^2/t = (20\ \mu m)^2/(10\ min) = 6.7 \times 10^{-13}\ m^2/s$. This value is roughly two orders of magnitude smaller than a typical small molecule diffusivity in dilute solution, thus suggesting that the interaction with the nanochannel wall decreases the diffusivity of the dye significantly.

The diffusion data of the oppositely charged dyes suggest that the nanochannel device could serve as a charge identifier for molecules whose charge status is unknown in certain conditions. In order to verify the idea, a zwitterion was tested. Texas red sulfonyl chloride (Molecular Probes) was chosen as the zwitterion counterpart to the sulforhodamine 101 cadaverine, allowing us to test the charge effect exclusively while maintaining other intrinsic properties. As shown in figure 4-6a, Texas red sulfonyl chloride has amine and sulfo functional groups as positive and negative charge sites, respectively. At this point, it proved to be very interesting to monitor the diffusion of the zwitterions through the nanochannel because both positive and negative sites must be strongly charged around neutral pH. The diffusion data for the zwitterion is presented in figure 4-6.

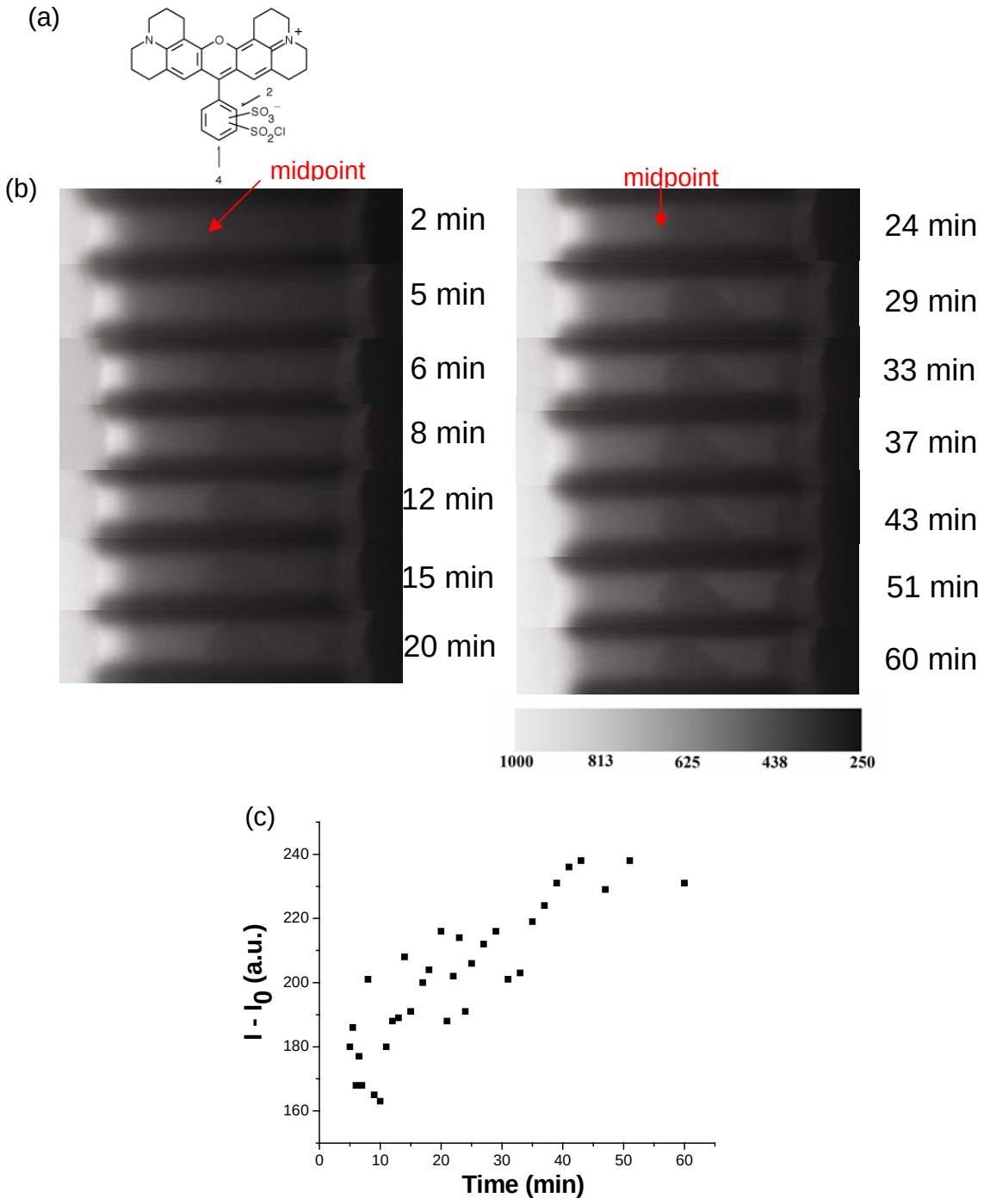

Figure 4-6. Diffusion of a zwitterionic dye. (a) Molecular structure of Texas red sulfonyl chloride used as a zwitterionic dye. (b) Fluorescence images over the nanochannel

regions taken during the diffusion. The dark spot in the middle of the nanochannel is believed to be a residue from the previous measurements. The channel width is about 4 μm. (c) Background subtracted fluorescence intensity measured at the midpoint of two different nanochannels.

The devices had to be recycled repeatedly for clear comparisons over the various dyes. In characterizing the zwitterionic dyes, in particular, the nanochannel appeared to have residues on the channel surface from the previous measurements, occurring as a dark spot in the middle of the channel (figure 4-6). Nevertheless, apparent diffusion was observed in the nanochannel, which suggests that the zwitterionic dye tested is not at least negatively charged. Because the zwitterionic dyes have two ionized sites of opposite polarities, it is expected that the dyes are more likely charged with either polarity rather than existing exactly neutral. From the observed diffusion, therefore, the net charge of the dye is expected to be positive. In order to test the hypothesis, biases of opposite polarities (±5 V) were applied sequentially while fluorescence images were taken periodically. Figure 4-7 presents those images and fluorescence intensity differences between both sides of microchannel. As shown in the figure, the dyes were driven toward lower potential sides at both bias applications. This electrophoretic transport validates the initial hypothesis that the dye is partially positively charged. Although further analysis is required to understand the origin of the partial charge, it could be presumed that the observed behavior is reflective of the fluidic environment inside the nanochannel where positive ions are dominant.

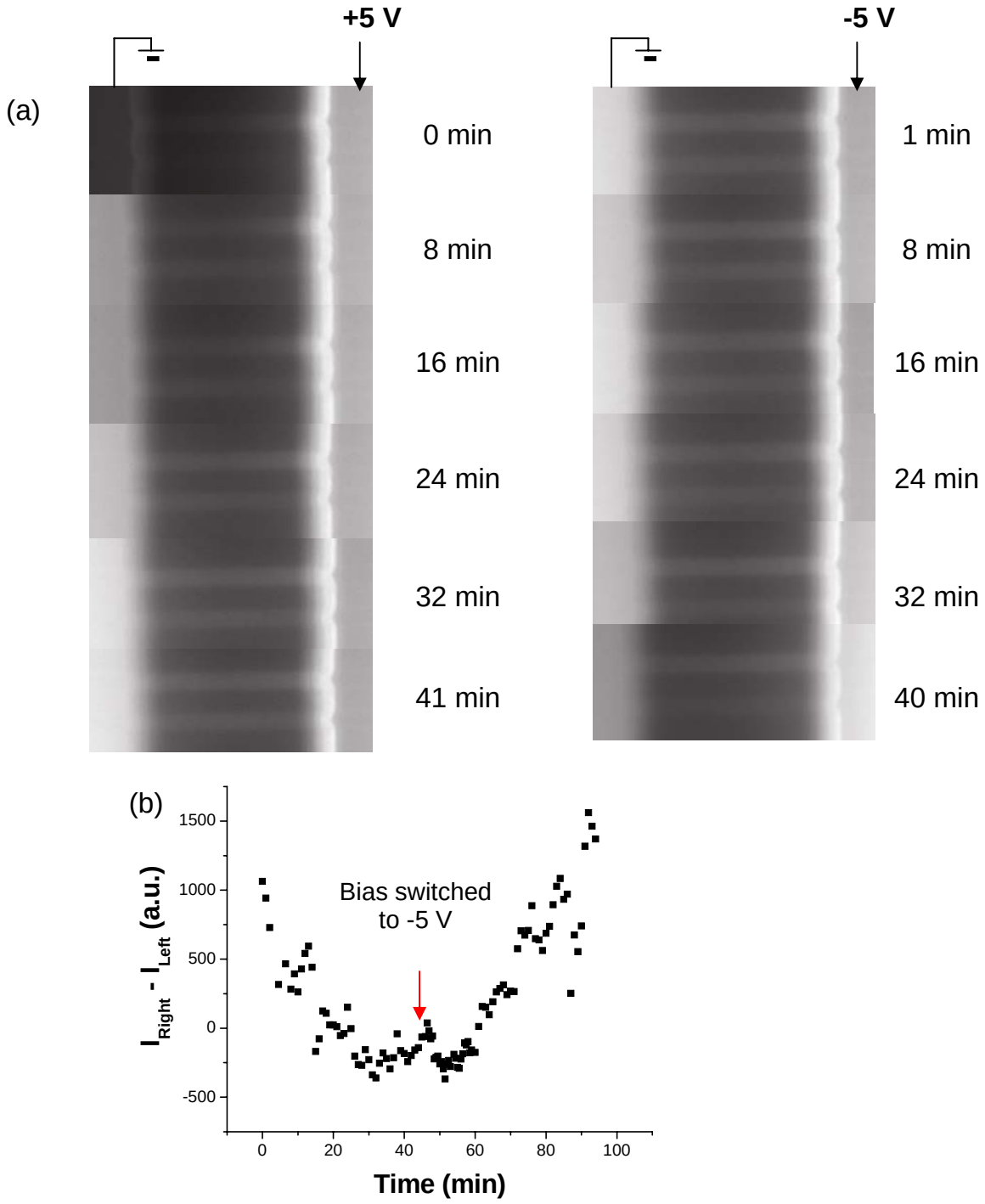

Figure 4-7. Bias measurements for the charge determination of the zwitterionic dye. (a) Positive (left panel) and then negative biases (right panel) are applied continuously to the right microchannel. It was visualized that the left microchannel becomes brighter

compared to the right one upon +5V application, whereas the brightness was switched upon -5 V application. (b) Fluorescence intensity difference between both sides of the microchannel. The point where the bias was switched to -5 V is indicated.

With nanoporous membranes, it is known that neutral molecules do not interact electrostatically with the surface of the membrane, thereby resulting in a larger flux across the membrane than charged molecules (15-18). In our measurements, the concentration difference between two specific points with regard to time should give diffusivity. Due to fabrication problems from the repeated device recycles, such as a minor leaking on the left side in figure 4-4, we require further measurements for a complete diffusivity analysis. The diffusivity analysis would provide better idea on the charge state of the zwitterionic dye by comparing its diffusivity against that of the cationic dye.

The charge-dependent diffusion not only indicates the unipolar characteristic of the nanochannel, but also implies that this platform could serve as a molecular separator or a charge identifier. The similar separation could be realized in a lower concentration of target molecules. Especially, by implementing a more sophisticated optical set-up, such as dark-field microscope that can image the target molecules attached to nanoparticles, the resolution of detecting the passage of the target molecules could be improved further. In summary, this technology suggests the possibility of a new type of column at a level close to single molecule resolution.

4.4 Conclusion and Future Work: Toward Quantification of Peptide Isoelectric Point via Gating Bias

Due to channel dimensions smaller than the Debye screening length, nanofluidics depicts interesting fundamental phenomena on ionic transport. Among those, the unipolar condition is most representative. Under the unipolar condition, the ions with different polarities should be considered separately because the surface charges on the nanochannel wall exert an opposite effect on those ions. To understand the system clearly, various parameters such as surface charge, ionic strength, external bias and charge-valency of carrying ions should be considered simultaneously because they are correlated to one another. The charge-dependent ionic diffusion has been observed via fluorescent dye molecules. The charge accumulation and depletion has been also observed upon external bias applicaiton. All results thus far can be explained within a consistent picture of a unipolar environment. Furthermore, the unipolar characteristic could be applied to separate molecules based on the charges as well as to identify the charge state of unknown molecules. Also, those applications should be possible for extremely small amounts of sample.

The project will be further expanded to detect a variety of target molecules including polymers, DNA and peptides. In device optimization, on the other hand, gating electrodes will be integrated over the nanochannel region to obtain a fine control over the surface charge. Among many candidates, the primary focus will be on quantification of peptide isoelectric points by adjusting the gating bias. About 5-mer length peptides, tagged with fluorescent dyes at the last residue, have been already synthesized by a manual coupling method. Fluorescence intensity will be obtained while the gating bias is

varied. The fluorescence intensity is expected to change most abruptly when the nanochannel surface charge, which is modulated by the gating bias, is close to the charge of target molecules. In other words, when half of the peptide population is positively charged and the other half is negatively charged, the change in fluorescence intensity would be most significant. Currently, two oppositely-charged polypeptides, such as polyaspartate and polylysine are being tested.

Once the idea is experimentally realized, its application would be multifold. One could separate a particular peptide from mixture by adjusting the gating bias. In addition, as a detection tool, the nanofluidic device could identify peptides based on the isoelectric points at a level close to a single molecule. Finally, its usage could be further extended to sequence proteins. Placing an unknown protein into solution within the nanochannels could allow the determination of its isoelectric point. The next step would be to enzymatically cleave the protein and flow the digested fragments through nanochannels, thereby determining the isoelectric points of the digested fragments. Repeating this procedure a few times would result in ascertaining the isoelectric points of many small peptides. Combining the knowledge of the amino-acid specific cleavage sites, in conjunction with the isoelectric point of the peptide fragments, the nanofluidic device should provide sufficient information to enable identification of the original protein. This would be an alternative to the more common mass spectrometry based method of peptide sequencing (19). The advantages of nanofluidics are that these devices could be operated in parallel and would require very little quantities of proteins, thus perhaps enabling protein discovery.

4.5 References

1. Kasianowicz, J. J., Brandin, E., Branton, D. & Deamer, D. W. (1996) *Proc. Nat. Acad. Sci.* 93, 13770-13773.
2. Howorka, S., Cheley, S. & Bayley, H. (2001) *Nat. Biotechnol.* 19, 636-639.
3. Fan, R., Karnik, R., Yue, M., Li, D. Y., Majumdar, A. & Yang, P. D. (2005) *Nano Lett.* 5, 1633-1637.
4. Karnik, R., Castelino, K., Fan, R., Yang, P. & Majumdar, A. (2005) *Nano Lett.* 5, 1638-1642.
5. Karnik, R., Fan, R., Yue, M., Li, D. Y., Yang, P. D. & Majumdar, A. (2005) *Nano Lett.* 5, 943-948.
6. Stein, D., Kruithof, M. & Dekker, C. (2004) *Phys. Rev. Lett.* 93.
7. Israelachvilli, J. (2003) *Intermolecular and surface forces,* Academic Press.
8. Fan, R., Yue, M., Karnik, R., Majumdar, A. & Yang, P. D. (2005) *Phys. Rev. Lett.* 95.
9. Stein, D., Kruithof, M. & Dekker, C. (2004) *Phys. Rev. Lett.* 93.
10. Karnik, R., Castelino, K., Fan, R., Yang, P. & Majumdar, A. (2005) *Nano Lett.* 5, 1638-1642.
11. Fu, J., Schoch, R. B., Stevens, A. L., Tannenbaum, S. R. & Han, J. (2007) *Nature Nanotechnol.* 2, 121-128.
12. Melosh, N. A., Boukai, A., Diana, F., Gerardot, B., Badolato, A., Petroff, P. M. & Heath, J. R. (2003) *Science* 300, 112-115.
13. Daiguji, H., Yang, P. D., Szeri, A. J. & Majumdar, A. (2004) *Nano Lett.* 4, 2315-2321.

14. Daiguji, H., Yang, P. D. & Majumdar, A. (2004) *Nano Lett.* 4, 137-142.

15. Burns, D. B. & Zydney, A. L. (1999) *Biotech. & Bioeng.* 64, 27-37.

16. Chun, K. Y. & Stroeve, P. (2002) *Langmuir* 18, 4653-4658.

17. Ku, J. R. & Stroeve, P. (2004) *Langmuir* 20, 2030-2032.

18. Lee, S. B. & Martin, C. R. (2001) *Anal. Chem.* 73, 768-775.

19. Wilm, M., Shevchenko, A., Houthaeve, T., Breit, S., Schweigerer, L., Fotsis, T. & Mann, M. (1996) *Nature* 379, 466-469.